Spin Density in a Nitronyl Nitroxide Free Radical. Polarized Neutron Diffraction Investigation and ab Initio Calculations[1]

Andrei Zheludev,[†] Vincenzo Barone,[‡] Michel Bonnet,[†] Bernard Delley,[§] André Grand,[∥] Eric Ressouche,[†] Paul Rey,*[,∥] Robert Subra,[⊥] and Jacques Schweizer*[,†]

Contribution from the Commissariat à l'energie atomique, MDN/SPSMS/DRFMC, CEN Grenoble, BP85X F-38041 Grenoble cêdex, France, Dipartimento di Chimica, Università Federico II, Via Mezzocannone 4, I-80134-Napoli, Italy, Paul Scherer Institute Zürich, Badenerstrasse 569, 8048 Zürich, Switzerland, Commissariat à l'energie atomique, SESAM/DRFMC, CEN Grenoble, BP85X F-38041 Grenoble cêdex, France, and LEDSS, Université Joseph Fourier, Avenue de la Chimie, BP35X, F-38041 Grenoble cêdex, France

Received March 29, 1993. Revised Manuscript Received December 8, 1993[⊛]

Abstract: The $P2_1/c$ form of the nitronyl nitroxide 2-phenyl-4,4,5,5-tetramethyl-4,5-dihydro-1*H*-imidazole-1-oxyl 3-oxide (NitPh) was investigated by conventional and polarized neutron diffraction. Model-free reconstruction of the spin distribution from the experimental structure factors using the recently developed 3D maximum of entropy technique gives the first direct experimental evidence for the p-shape of the spin density in the vicinity of the major spin carriers in nitroxide free radicals. Using other reconstruction methods gives individual atomic spin populations. Most of the spin density is equally shared between the four atoms of the two NO groups. In addition, the bridging sp^2 carbon atom carries a significant negative spin density. Delocalization of the unpaired spin onto the phenyl fragment is weak; sign alternation on the ring is observed and agrees with previous NMR experiments. The experimental results are compared to those obtained by various theoretical *ab initio* calculations. Unrestricted Hartree–Fock (UHF), second order Moller–Plesset (MP2), and complete configuration interaction (CI) calculations predict correctly the signs of individual atomic spin populations, but as long as the magnitudes are concerned, the agreement with experiment is rather poor. Nevertheless, the results are improved significantly in going from UHF to MP2 and CI as the correlation energy is better accounted for. On the contrary, density functional theory (DFT) calculations give good results for both the signs and magnitudes of spin populations and require much less computation time and system resources. The role of the basis set was also studied. UHF is improved by using a larger basis set. The choice of a suitable basis is thus crucial. Unlike the case of UHF, DF results are quite stable with respect to the basis set used, and a rather limited one is sufficient.

Introduction

The spin-labeling technique[2,3] strongly contributed to the development of the organic chemistry of nitroxide free radicals.[4,5] Recently however, much of the impetus for these paramagnetic species stems from their use as building blocks in magnetic molecular materials.[6,7] Indeed, nitroxides and particularly nitronyl nitroxides have proven to be versatile building blocks for the design of purely organic materials[8,9] and mixed coordination complexes[4] as well. Examples of both types of materials have been characterized which exhibit bulk ferromagnetism at low temperature. Much of the current work in this field is aimed at understanding the coupling mechanisms and, correlatively, at increasing the transition temperatures.

In nitroxide–metal complexes, interactions between directly bound spin carriers are fairly well modeled using local parameters in the frame of Heitler–London theory. However, strong exchange interaction arises when the distances between interacting centers become sufficiently small. In this case the different sites may lose their individuality and the spin density distribution may be changed dramatically. Such a modification has been observed by an experimental study by polarized neutron diffraction in two nitronyl nitroxide–copper(II) complexes.[10] These studies showed that unpaired spin distribution in a coordinated nitroxide ligand is strongly dependent on the coordination geometry and is strongly correlated to the magnitude of exchange interaction, being very different from that predicted by elementary Molecular Orbital theory. In order to get a quantitative description of the changes arising upon coordination in a nitronyl nitroxide ligand, we have performed a spin distribution determination on an uncoordinated nitroxide 2-phenyl-4,4,5,5-tetramethyl-4,5-dihydro-1*H*-imidazol-1-oxyl 3-oxide (NitPh, Figure 1).

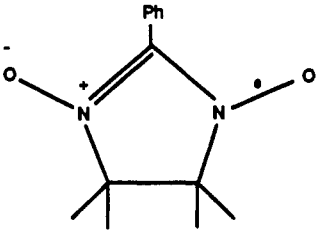

Figure 1. Chemical structure of NitPh.

This phenyl-substituted nitroxide has been widely used as ligand toward paramagnetic metal ions,[8] and it is the most popular representative of the nitronyl nitroxide family,[11] which includes the *p*-nitrophenyl nitronyl nitroxide, the first reported purely

† MDN/SPSMS/DRFMC.
‡ Universitá Federico II.
§ Paul Scherer Institute Zürich.
∥ SESAM/DRFMC.
⊥ Université Joseph Fourier.

⊛ Abstract published in *Advance ACS Abstracts*, February 1, 1994.

(1) Part of the thesis work of A. Zheludev.
(2) Stone, T. J.; Buckman, T.; Nordio, P. L.; McConnel, H. *Proc. Natl. Acad. Sci. U.S.A.* **1965**, *54*, 1010.
(3) Berliner, L. D., Ed. *Spin Labeling*; Academic Press: New York, 1976 (Vol. 1), 1979 (Vol. 2).
(4) Rozantsev, E. G. *Free Nitroxyl Radicals*; Plenum Press: New York, 1970.
(5) Keana, J. F. *Chem. Rev.* **1978**, *78*, 37.
(6) Caneschi, A.; Gatteschi, D.; Sessoli, R.; Rey, P. *Acc. Chem. Res.* **1989**, *22*, 392.
(7) Caneschi, A.; Gatteschi, D.; Rey, P. *Prog. Inorg. Chem.* **1991**, *39*, 331.
(8) Awaga, K.; Maruyama, Y. *Chem. Phys. Lett.* **1989**, *158*, 556.
(9) Kinoshita, M.; Turek, P.; Tamura, M.; Nozava, K.; Shiomi, D.; Nakazava, Y.; Ishikawa, M.; Takahashi, M.; Awaga, K.; Inabe, T.; Maruyama, Y. *Chem. Lett.* **1991**, 1225.
(10) Ressouche, E.; Boucherle, J.-X.; Gillon, B.; Rey, P.; Schweizer, J. *J. Am. Chem. Soc.* **1993**, *115*, 3610.
(11) Ullman, E. F.; Osiecki, J. H.; Boocock, D. G. B.; Darcy, R. *J. Am. Chem. Soc.* **1972**, *94*, 7049.

0002-7863/94/1516-2019$04.50/0

organic ferromagnet.[9] Thanks to two sites of coordination, these compounds led to an interesting series of unidimensional materials.[12,13] Trends toward compounds of higher dimensionality which would exhibit bulk ferromagnetic properties at higher temperature involve nitroxides substituted by aromatic groups carrying donor atoms.[14,15] The knowledge of the spin density distribution in the phenyl analogue will provide a crude quantitative frame for understanding exchange interactions in complexes of these ligands.

Another interest in the experimental determination of the spin density distribution in NitPh was not only to compare density maps in coordinated and uncoordinated ligands but also to bring experimental reference to several theoretical calculations. Using commercially available software, we have investigated which level of approximation is appropriate to give reliable results.

Neutrons, thanks to their magnetic moments, make a perfect tool for spin density studies.[16] On the one hand they can be used to measure microscopic distributions of spin densities as opposed to bulk magnetization and susceptibility measurements. On the other hand, unlike the resonance techniques that are restricted to measuring the spin densities at certain sites in the molecule by virtue of magnetic probes fixed to the molecular skeleton, neutrons are itinerant probes, giving information on spin density at every point of the sample.

Neutrons are scattered in a magnetic crystal by means of nuclear interaction with the nuclei and magnetic interaction with the magnetization (spin) density. If the temperature is not very low ($T > \sim 1$ K), even in a strong magnetic field ($H \sim 5$ T), the nuclear spins are not polarized and the nuclear scattering is independent of the neutron spin. On the contrary, the interaction of the neutron with the magnetization density can be treated as a dipole–dipole interaction and is of course spin-dependent. This allows us to separate the magnetic and the nuclear signals by using a polarized neutron beam and performing measurements for different beam polarizations.

The structure factor $\vec{F}_M(\vec{q})$ for magnetic scattering ($\vec{q}$ being the scattering vector) is a vector quantity proportional to $\vec{M}(\vec{q})$, the Fourier component of the magnetization density $\vec{M}(\vec{r})$ in the crystal:

$$\vec{F}_M(\vec{q}) = r_0 \vec{M}(\vec{q}) = r_0 \int \vec{M}(\vec{r}) e^{i(\vec{q}\cdot\vec{r})} d^3\vec{r} \qquad (1)$$

$$r_0 = 0.2696 \times 10^{-12} \text{ cm}/\mu_B$$

The expression for total (nuclear and magnetic) scattered intensity for the case when no polarization analysis is performed and the incident neutron beam is polarized, $\vec{\sigma}$ being the polarization direction, is given by

$$I(\vec{q},\vec{\sigma}) = |F_N|^2 + |\vec{F}_{M_\perp}|^2 + F_N(\vec{\sigma}\cdot\vec{F}^*_{M_\perp}) + F^*_N(\vec{\sigma}\cdot\vec{F}_{M_\perp}) \qquad (2)$$

$$\vec{F}_{M_\perp} = \hat{q} \times \vec{F}_M \times \hat{q}; \quad \hat{q} = \frac{\vec{q}}{|\vec{q}|}$$

where the F_N's are the nuclear scattering amplitudes (structure factors).

Polarized neutron diffraction studies of a paramagnetic single crystal imply inducing a magnetization density by means of a strong magnetic field at low temperature. The induced magnetization density is periodic just as the nuclear density. For this reason all the coherent elastic scattering occurs at the Bragg scattering positions for which $\vec{q}$ is an integer reciprocal lattice vector (hkl). For an isotropic paramagnet the induced magnetization density is aligned with the applied field. This reduces $\vec{M}(\vec{r})$ and hence $\vec{F}_M(\vec{q})$ to scalar functions: $\vec{F}_M(\vec{q}) = \hat{z}F_M(\vec{q})$, $\hat{z}$ being a unit vector along the applied field. Furthermore, if the structure is centrosymmetric, both $\vec{F}_M$ and F_N are real quantities. One measures the so-called flipping ratio R of Bragg reflections—the ratio of the scattered intensities for the polarization of the incident neutron beam parallel ('up') and antiparallel ('down') to the applied magnetic field. Using the general formula (1) the expression for R is obtained as

$$R(h,k,l) = \frac{I^\uparrow}{I_\downarrow} = \frac{F_N^2 + F_{M_\perp}^2 + 2F_N F_{M_{\perp z}}}{F_N^2 + F_{M_\perp}^2 - 2F_N F_{M_{\perp z}}} \qquad (3)$$

$$\vec{F}_M = \hat{z}F_M; \quad F_{M_\perp} = F_M \sin\alpha; \quad F_{M_{\perp z}} = F_M \sin^2\alpha$$

where α is the angle between the scattering vector (hkl) and $\hat{z}$.

Given the F_N's one can obtain the magnetic structure factors from the flipping ratios by solving (3) and use them to reconstruct the spatial spin density, solving the inverse Fourier problem. The nuclear structure factors can be calculated if the precise structure of the crystal is known. Thus the experiment has to include two steps. In the first step the structure of the crystal is determined using conventional unpolarized neutron diffraction techniques. The second step is devoted to measuring the flipping ratios (polarized neutrons).

Table 1. Crystal Data and Experimental Parameters for the Unpolarized Neutron Experiment

temperature	6 K
neutron wavelength	1.138 Å
no. of independent reflections	1320
space group	$P2_1/c$
cell constants	$a = 20.871(13)$ Å
	$b = 10.150(09)$ Å
	$c = 12.130(21)$ Å
	$\beta = 107.15(10)°$
$\sin\theta/\lambda_{max}$	0.48 Å^{-1}
R factors	$R(F) = 0.0794$
	$R(F^2) = 0.742$
	$R_w(F) = 0.0620$

Experimental Section

The synthesis and physical properties of NitPh have been reported elsewhere.[17] The room temperature structure for NitPh is known from X-ray analysis.[18] Large crystals suitable for neutron diffraction experiments were grown by slow evaporation of concentrated hexane–methylene chloride (50/50) solutions in the dark at room temperature.

Low-Temperature Structure Determination. The single crystal of dimensions $4 \times 2.5 \times 1$ mm^3 that we used for the neutron experiment was in the form of a regular slab. It was preliminarly oriented by Laue X-ray diffraction. The neutron diffraction experiment was conducted on the DN4 four-circle diffractometer at the reactor SILOE at the Centre d'Etudes Nucléaires de Grenoble (France). A three-stage Joule–Thompson refrigerator was used to cool the sample down to 6 K. Crystal data are reported in Table 1 with pertinent experimental parameters.

The calculation of integrated intensities from the ω-scans was done by the COLL5 program[19] during experimental run time. For the averaging of equivalent reflections, the program ARRNGE based on the Cambridge Crystallographic Library[20] was used. The absorption coefficient $\mu = 0.22$ mm^{-1} was obtained from the empirical chemical formula and the mean inelastic cross sections for each element. It was then used to calculate the absorption correction by estimating the mean crystal-traversing path for each (hkl) reflection collected. No extinction corrections were made.

(12) Caneschi, A.; Gatteschi, D.; Renard, J.-P.; Rey, P.; Sessoli, R. *Inorg. Chem.* **1989**, *28*, 1976.
(13) Caneschi, A.; Gatteschi, D.; Renard, J.-P.; Rey, P.; Sessoli, R. *Inorg. Chem.* **1989**, *28*, 2940.
(14) Caneschi, A.; Farraro, F.; Gatteschi, D.; Rey, P.; Sessoli, R. *Inorg. Chem.* **1990**, *29*, 1756.
(15) Caneschi, A.; Ferraro, F.; Gatteschi, D.; Rey, P.; Sessoli, R. *Inorg. Chem.* **1990**, *29*, 4217.
(16) Gillon, B.; Schweizer, J. Study of Chemical Bonding in Molecules: The interest of Polarized Neutron Diffraction. In *Molecules in Physics, Chemistry and Biology*; Jean Maruani, Ed.; Kluwer Academic Publisher: Dordrecht, The Netherlands, 1989; Vol. II, p 111.
(17) Osiecki, J. H.; Ullman, E. F. *J. Am. Chem. Soc.* **1968**, *90*, 1078.
(18) Wong, W.; Watkins, S. F. *J. Chem. Soc., Chem. Commun.* **1973**, 888.
(19) Lehmann, M. S.; Larsen, F. K. *Acta Crystallogr.* **1970**, *B26*, 1198.
(20) Brown, P. J.; Matthewman, J. C. *The Cambridge Crystallographic Subroutine Library* RL-81–063.

Table 2. Selected Low-Temperature Bond Lengths (Å) and Angles (deg)

O1–N1	1.259(6)	O1–N1–C7	127.05(5)
O2–N2	1.272(7)	O2–N2–C7	127.8(5)
N1–C7	1.345(7)	O1–N1–C8	120.8(5)
N2–C7	1.364(5)	O2–N2–C9	121.7(4)
C8–N1	1.511(6)	N1–C7–N2	109.3(4)
C9–N2	1.538(8)	N1–C8–C9	101.6(4)
C8–C9	1.525(7)	N2–C9–C8	100.3(4)
C7–C6	1.488(8)	N1–C8–C10	110.3(6)
C6–C1	1.398(6)	N1–C8–C11	104.9(5)
C1–C2	1.389(8)	N2–C9–C12	106.6(4)
C2–C3	1.370(9)	N2–C9–C13	108.1(6)
C3–C4	1.397(8)	C9–C8–C10	115.9(6)
C4–C5	1.405(8)	C9–C8–C11	113.9(6)
C5–C6	1.393(9)	C8–C9–C12	114.9(6)
C8–C10	1.500(9)	C8–C9–C13	115.5(4)
C8–C11	1.552(9)	N1–C7–C6	125.8(4)
C9–C12	1.514(9)	N2–C7–C6	125.0(5)
C9–C13	1.525(7)	O3–N3–C20	125.7(4)
O3–N3	1.278(8)	O4–N4–C20	126.8(4)
O4–N4	1.269(8)	O3–N3–C21	122.2(5)
N3–C20	1.335(6)	O4–N4–C22	123.0(5)
N4–C20	1.374(7)	N3–C20–N4	108.6(4)
C21–N3	1.502(5)	N3–C21–C22	100.2(5)
C22–N4	1.488(5)	N4–C22–C21	102.1(5)
C21–C22	1.525(9)	N3–C21–C23	105.3(5)
C20–C14	1.463(6)	N3–C21–C24	112.7(4)
C14–C15	1.406(9)	N4–C22–C25	111.3(4)
C15–C16	1.380(7)	N4–C22–C26	105.0(5)
C16–C17	1.388(9)	C22–C21–C23	109.8(5)
C17–C18	1.395(9)	C22–C21–C24	119.6(6)
C18–C19	1.391(7)	C21–C22–C25	120.1(6)
C19–C14	1.394(9)	C21–C22–C26	109.6(5)
C21–C23	1.582(10)	N3–C20–C14	127.6(5)
C21–C24	1.471(9)	N4–C20–C14	123.7(5)
C22–C25	1.501(9)		
C22–C26	1.564(7)		

Refinement of the atomic positions from room-temperature values was done with the least-squares program ORXFLS[21] using isotropic thermal factors for all atoms. Refinement statistics are also presented in Table 1. Table 2 lists selected interatomic distances and bond angles. Figure 2 presents the two molecules and the atom-labeling scheme used throughout the paper. The complete atom-labeling scheme (Figure S1), a picture showing the positions of the molecules with respect to the unit cell (Figure S2), atomic fractional cell coordinates and isotropic thermal parameters (Table S1), and complete tables of bond lengths (Table S2) and angles (Table S3) are deposited as supplementary material.

Polarized Neutron Experiment. The polarized neutron investigation of the compound included two series of experiments. In the first series a crystal of size 10 × 4.5 × 1.3 mm³ was mounted on the DN2 polarized neutron diffractometer at SILOE with the $\vec{c}$ axis vertical, parallel to the applied H = 8 T magnetic field of a cryomagnet. The construction of the superconducting coil and the use of a lifting counter enables one to measure several planes in reciprocal space: reflections of type ($hk0$), ($hk1$), and ($hk2$) were accessible for measurements. In the second series of experiments the same crystal was used, but it was remounted to have the $\vec{b}$ axis vertical, aligned with the field H = 4.65 T in another cryomagnet. Reflections of type ($h0l$), ($h1l$), and ($h2l$) were measured. In both series the sample temperature, T = 5 K, was maintained. Altogether 254 independent flipping ratios were collected with maximum $\sin\theta/\lambda = 0.42$ Å^{-1}, the incident wavelength was 1.25 Å.

The nuclear structure factors were calculated from the previously determined crystal structure using the ORXFLS program. The subroutine library mentioned above was used to sort and average equivalent flipping ratios. The F_M values were calculated from the flipping ratios taking into account the beam polarization, the flipping efficiency, and the $\lambda/2$ beam contamination. Note that absorption corrections do not have to be made in the flipping ratio measurement method and that the experimental temperature is high enough to make nuclear spin polarization contributions to the magnetic signal negligible.

Magnetic Measurements. To make clear the magnetic behavior of NitPh and to obtain the magnetic structure factor of the (000) reflection which allows one to scale the results of the two experiments conducted at different applied fields, magnetic investigations of 32.1 mg of NitPh powder were done on a commercial Quantum Design SQUID magnetometer. The dc-susceptibility $\chi(T)$ in a constant applied field of 0.5 T in the range 2–300 K and the magnetization $M(H)$ at a constant temperature of 5 K and fields up to 5.5 T were investigated. The Brillouin function $B_{1/2}$ with spin $^1/_2$ per NitPh molecule fits both curves perfectly. Corresponding magnetization values are 0.79 μ_B/NitPh for the first polarized neutron experiment (H = 8 T, T = 5 K) and 0.56 μ_B/NitPh for the second one (H = 4.65 T, T = 5 K). The F_M's obtained in the two experiments were scaled to H = 8 T, T = 5 K.

(21) Busing, W. R.; Martin, K. O.; Levy, H. A. Rapport O.R.N.L. 59-4-37; Oak Ridge National Laboratory: Oak Ridge, TN, 1991.

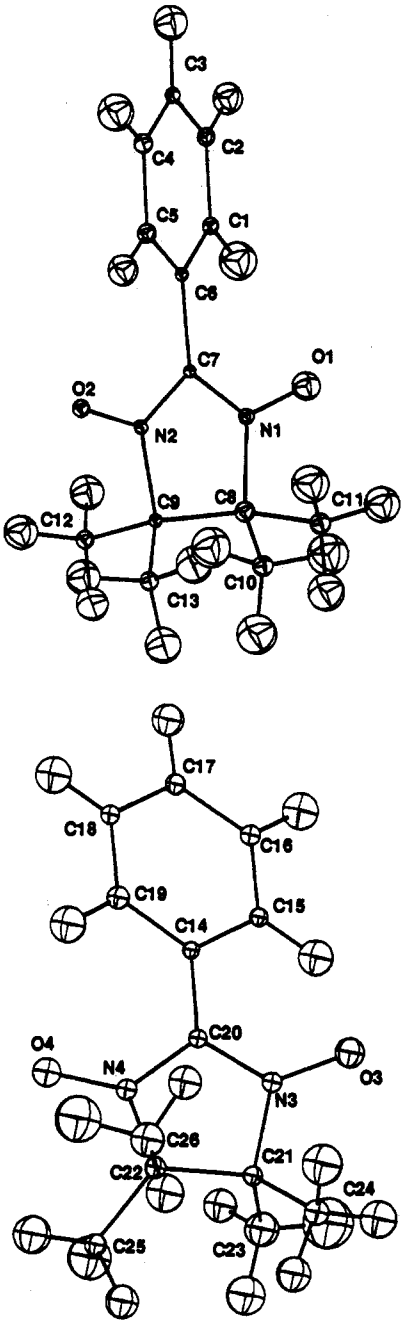

Figure 2. View of the two independent molecules showing the numbering scheme of the atoms: (a) first molecule; (b) second molecule.

Data Treatment and Results

Structural Study. At low temperature the crystal symmetry is preserved and no drastic changes in cell constants are observed. The O–N–C–N–O conjugate fragment remains nearly perfectly planar and symmetrical. The planes of the phenyl fragments are rotated with respect to the O–N–C–N–O planes by the angles 24.5° and 29.8° around the C7–C6 and C14–C20 bonds in the first and second molecule, respectively. The corresponding angles at room temperature are similar: 25.9° and 31.5°.

Spin Density Reconstruction. Reconstruction of the spatial spin density $S(\vec{r})$ from the magnetic structure factors F_M's is a typical inverse Fourier problem. It has to be solved taking heed of the specific problems which limit the accuracy and completeness of polarized neutron diffraction data. Firstly, the limitation in $\sin\theta/\lambda$ is the limitation in the spatial resolution of the experiment. This is a general problem encountered in diffraction. Secondly, the construction of the cryostat and the superconducting coil make a large part of the Fourier space inaccessible for measurements. This is aggravated by the geometrical factor $\sin\alpha$ in eq 3—the magnetic signal is decreased when the counter is lifted from the horizontal plane. Even though this problem is partially solved by the successive mounting of the crystal in two different orientations, the detector still cannot be positioned for some Bragg reflections. The third group of problems arises from the fact that F_M's, which are much smaller than F_N's ($|F_M| \ll |F_N|$), can be measured by polarized neutrons only thanks to the amplifying effect of the nuclear structure factors. As a result, for small F_N's the Bragg peaks can be lost in the background even if the corresponding magnetic scattering is relatively large. For those F_M's which can be measured, this causes the error bars to be very uneven. Thus we end up with a scarce and somewhat arbitrary sampling of data points in Fourier space. Several approaches to solving the inverse Fourier (IF) problem were used.

Model-Independent Spin Density. Model-independent methods allow one to reconstruct the spin density without involving any *a priori* knowledge of what the spin density should look like. Applying them is very important to test the models and to judge the quality of the data obtained. The most straightforward approach to solving the IF problem is to calculate the inverse Fourier sum

$$S(x,y,z) = 1/V\sum_{h,k,l} F_M(h,k,l)e^{-2\pi i(hx+ky+lz)} \qquad (4)$$

where V is the unit cell volume. The sum is taken over all Bragg reflections for which the F_M's were determined. This method has been widely used to interpret polarized neutron diffraction data, but it has its drawbacks. Since not all Fourier components are known, there are in fact many possible three-dimensional spin density distributions (maps) which fit the data. Fourier inversion selects one of them—the one with zero values for unmeasured coefficients and values exactly in the middle of the error bars for those measured. On the contrary, the recently developed maximum of entropy (ME) technique[22] selects among all the maps consistent with the data the most probable one, that is the one which maximizes the Boltzman entropy:

$$\text{entropy}(S(\vec{r})) = -\int_{\text{unit cell}} s(\vec{r}) \ln(s(\vec{r}))\mathrm{d}^3\vec{r}$$

$$s(\vec{r}) = \frac{S(\vec{r})}{\int_{\text{unit cell}} S(\vec{r})\ \mathrm{d}^3\vec{r}} \qquad (5)$$

This formula applies to strictly positive densities, but the method is easily modified to treat sign-alternating densities. In practice one maximizes the functional (5) calculated for a three-dimensional spin density map under the constraints $\chi^2 \leq 1$. A projection along the desired direction is obtained directly by integrating the three-dimensional density. One is no longer restricted to the reconstruction of a projection onto a plane for which enough Fourier components are known. Once the MaxEnt principle is assumed, even the out-of-plane reflections contribute to the reconstruction of a projection.[23] This method is known to give much better results than conventional Fourier inversion and is also model-independent.

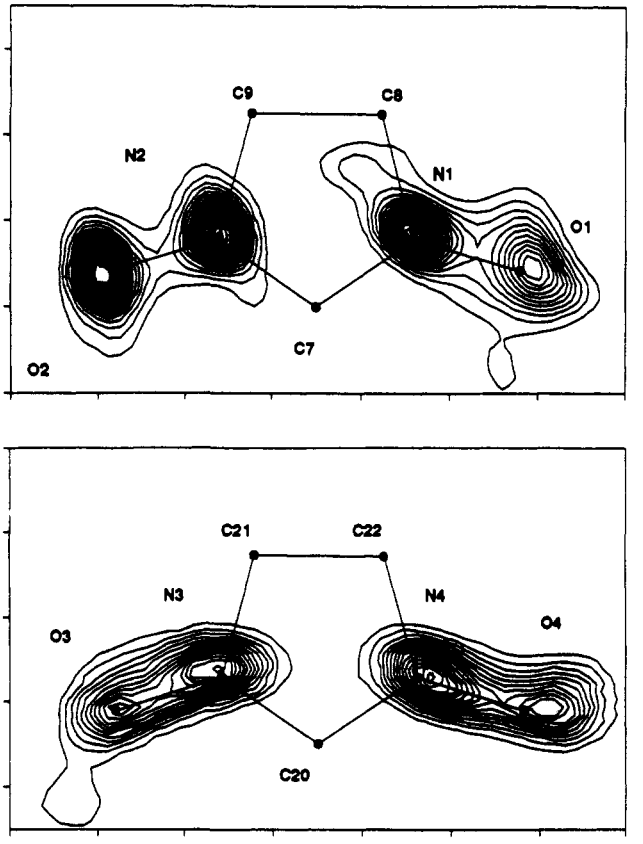

Figure 3. Projection of the MaxEnt reconstructed spin density onto the nitroxide mean plane: Contour step 0.02 $\mu_B/Å^2$; (a) first molecule; (b) second molecule.

Figure 3 shows the projection of the MaxEnt reconstructed spin density onto the molecular O–N–C–N–O planes of the two molecules. Figure 4 shows the projection onto the plane which is parallel to the N–N direction and perpendicular to the O–N–C–N–O plane. These reconstructions show that most of the spin is carried by the oxygen and nitrogen atoms. They confirm the equivalence on the two NO groups of each NitPh molecule. Moreover, one can see the p-shape of the magnetic molecular orbital (Figure 4). On one of the nitrogen atoms one distinctly sees two spin density maxima, and though the maxima are not visible for the other atoms, the spin density cloud is stretched along the direction perpendicular to the O–N–C–N–O plane. One can hardly hope to obtain better direct experimental evidence for the π^*-shape of the magnetic orbital with the experimental resolution available.

MaxEnt also suggests that the spin density is evenly shared by the N and O atoms within each NO group. Even though no spin is detected on atoms of the carbon skeleton, this cannot be used as evidence for the absence of spin population on these sites. MaxEnt is usually capable of locating only the strong contributions to the spin density, smoothing out the weak peaks as long as this is permitted by the experimental data.

Probably this is the first time a magnetic π^*-orbital is 'seen' without introducing the p-shape of atomic orbitals into the data treatment as *a priori* information. The high quality of the reconstructions shows the power of the 3D MaxEnt approach.

Modeling the SpinDensity. To obtain individual populations and to try to extract some information on the spin density of thecarbon molecular skeleton and the phenyl fragment, the magnetic wave-function refinement method was used.[16] In this framework a Hartree–Fock style magnetic wave function $|\psi_i\rangle$ is

(22) Papoular, R. J.; Gillon, B. *Europhys. Lett.* **1990**, *13*, 429.
(23) Papoular, R. J.; Ressouche, E.; Schweizer, J.; Zheludev, A. In *Fundamental Theories in Physics*, Volume 53, *Maximum Entropy And Bayesian Methods*; Mohammad-Djafari, A., Demoment, G., Ed.; Kluver Academic Press: 1993; pp 311–318.

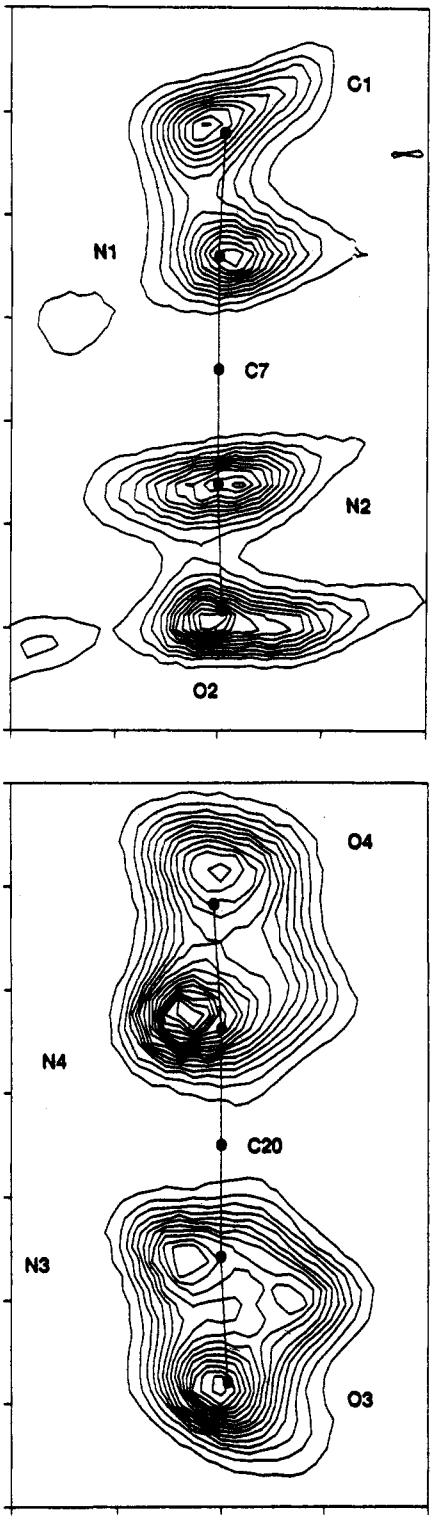

Figure 4. Projection of the MaxEnt reconstructed spin density onto a plane perpendicular to the nitroxide mean plane: (a) first molecule, contour step 0.02 $\mu_B/Å^2$; (b) second molecule, contour step 0.01 $\mu_B/Å^2$.

constructed from standard Slater atomic orbitals at each atomic site i:

$$|\psi_i\rangle = \sum_j \alpha_{i,j}|\phi_j\rangle$$

In this formula j labels the atomic Slater wave functions and ϕ_j and $\alpha_{i,j}$ are the expansion coefficients. To allow for both positive- and negative-spin populations, the spin density $S(\vec{r})$ is expanded as

$$S(\vec{r}) = \sum_i S_i \psi_i(\vec{r})\psi^*{}_i(\vec{r})$$

Table 3. Atomic Spin Populations Corresponding to T = 5 K, H = 8 T

atom	orbital	population
O2	$\|2p_x\rangle$, $\|2p_y\rangle$, $\|2p_z\rangle$	0.223(9)
N2	$\|2p_x\rangle$, $\|2p_y\rangle$, $\|2p_z\rangle$	0.199(8)
C7	$\|2s\rangle$	−0.073(11)
N1	$\|2p_x\rangle$, $\|2p_y\rangle$, $\|2p_z\rangle$	0.203(10)
O1	$\|2p_x\rangle$, $\|2p_y\rangle$, $2p_z\rangle$	0.190(9)
C8	$\|2s\rangle$	−0.022(12)
C9	$\|2s\rangle$	0.003(10)
C10	$\|2s\rangle$	0.029(9)
C11	$\|2s\rangle$	0.011(9)
C12	$\|2s\rangle$	0.032(10)
C13	$\|2s\rangle$	−0.004(9)
C1	$\|2p_{z'}\rangle$	0.009(10)
C2	$\|2p_{z'}\rangle$	0.001(11)
C3	$\|2p_{z'}\rangle$	−0.019(9)
C4	$\|2p_{z'}\rangle$	−0.002(8)
C5	$\|2p_{z'}\rangle$	−0.024(10)
C6	$\|2p_{z'}\rangle$	0.008(11)
total		0.761(40)
O4	$\|2p_x\rangle$, $\|2p_y\rangle$, $\|2p_z\rangle$	0.208(10)
N4	$\|2p_x\rangle$, $\|2p_y\rangle$, $\|2p_z\rangle$	0.209(11)
C20	$\|2s\rangle$	−0.091(13)
N3	$\|2p_x\rangle$, $\|2p_y\rangle$, $\|2p_z\rangle$	0.209(12)
O3	$\|2p_x\rangle$, $\|2p_y\rangle$, $\|2p_z\rangle$	0.186(10)
C21	$\|2s\rangle$	−0.019(12)
C22	$\|2s\rangle$	0.007(10)
C23	$\|2s\rangle$	0.041(9)
C24	$\|2s\rangle$	0.007(10)
C25	$\|2s\rangle$	−0.006(9)
C25	$\|2s\rangle$	−0.004(10)
C15	$\|2p_{z'}\rangle$	0.000(10)
C16	$\|2p_{z'}\rangle$	0.019(10)
C17	$\|2p_{z'}\rangle$	−0.012(9)
C18	$\|2p_{z'}\rangle$	0.008(9)
C19	$\|2p_{z'}\rangle$	−0.028(10)
C14	$\|2p_{z'}\rangle$	0.018(12)
total		0.752(51)

The coefficients $\alpha_{i,j}$ are scaled to give $\langle\psi_i|\psi_i\rangle = 1$. The individual atomic populations S_i as well as the coefficients $\alpha_{i,j}$ and the radial exponents of the Slater wave functions for each orbital type are the parameters of the model which are refined to best fit the data.

For the particular case of NitPh, theoretical considerations and MaxEnt results suggest to include the $|2p\rangle$ orbitals at the N and O atomic sites. The $|2p_x\rangle$, $|2p_y\rangle$, and $|2p_z\rangle$ (axis z is perpendicular to the O–N–C–N–O plane of each molecule) orbitals were included in the refinement, yielding $|\psi\rangle = \alpha_1|2p_x\rangle + \alpha_2|2p_y\rangle + \alpha_3|2p_z\rangle$, $\alpha_1^2 + \alpha_2^2 + \alpha_3^2 = 1$. The spin density on the carbon atoms of NitPh is not revealed by MaxEnt and therefore is weak and can be reduced to spherical contributions except on the bridging carbon atom, where $|2p_z\rangle$ orbitals were used. $|2p_{z'}\rangle$ orbitals make a reasonable choice for the phenyl carbon sites, axis z' being perpendicular to the phenyl ring plane.

The refinement was done using a modification of the least-squares program MOLLY.[24] The starting values of the Slater radial exponents were taken from ref 25. They were refined for the N and O but not for C atoms, since the spin density is less significant on the latter. The resulting populations for both molecules are presented in Table 3. Table 4 shows the refined α_{ij} coefficients for the $|2p_x\rangle$, $|2p_y\rangle$, and $|2p_z\rangle$ orbitals on the N and O sites and the refined values of the radial exponents. The statistics of the refinement are presented in Table 5. Figure 5 shows the higher level contours for the spin density projected onto the O–N–C–N–O plane of the two NitPh molecules. Only the low-level contours are shown on Figure 6. Figure 7 shows the reconstructed spin density projected onto the plane which is perpendicular to the O–N–C–N–O plane and parallel to the N–N

(24) Hansen, N. K.; Coppens, P. *Acta Crystallogr.* **1978**, *A34*, 909.
(25) Hehre, N. J.; Stewart, R. F.; Pople, J. A. *J. Chem. Phys.* **1969**, *51*, 2657.

Table 4. Refined Wave Function Coefficients $\alpha_{i,j}$ and Slater Radial Exponents

atom	α_1 ($\|2p_x\rangle$)	α_2 ($\|2p_y\rangle$)	α_3 ($\|2p_z\rangle$)	atom type	Slater exponent
O1	0.23(19)	0.41(25)	0.88	C	3.44 (not refined)
N1	0.10(16)	0.27(22)	0.96	N	4.45(17)
N2	0.00(14)	0.00(23)	1.00	O	4.50(19)
O2	−0.21(15)	−0.07(16)	0.98		
O3	0.23(18)	−0.10(15)	0.97		
N3	0.02(20)	0.17(17)	0.99		
N4	0.12(18)	0.18(14)	0.98		
O4	−0.12(18)	0.25(16)	0.96		

Table 5. Wave Function Refinement Statistics

no. of variables	52
no. of independent F_M's	254
χ^2/N_{obs}	1.58
weighted crystallographic r factor	14.55%

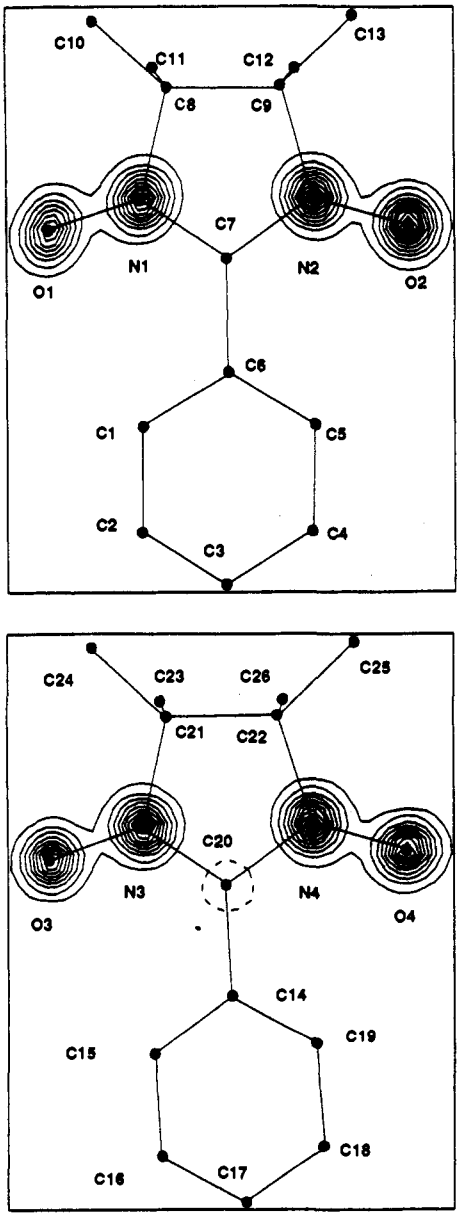

Figure 5. Projection onto the nitroxide mean plane of the high-level contours (step 0.1 $\mu_B/Å^2$) of the spin density as analyzed by wave-function modeling. The zero-level contour is not shown. Negative contours are dashed: (a) first molecule; (b) second molecule.

direction. The total populations of the NitPh molecules (0.761(40) and 0.752(51) μ_B/NitPh) obtained by the refinement are in good agreement with magnetization results (0.79 μ_B/NitPh).

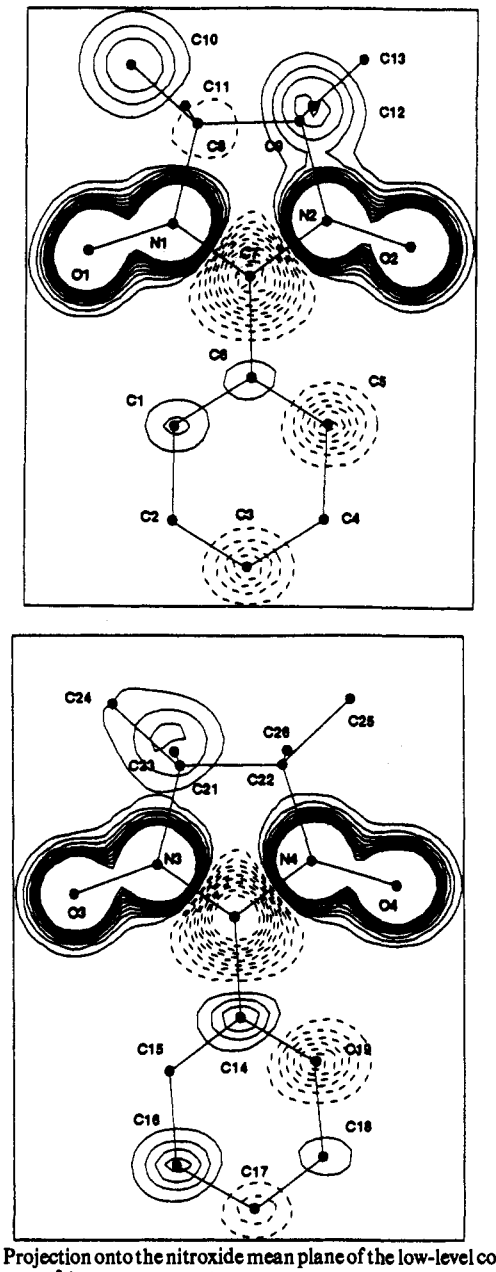

Figure 6. Projection onto the nitroxide mean plane of the low-level contours (step 0.01 $\mu_B/Å^2$) of the spin density as analyzed by wave-function modeling. The zero-level contour is not shown. Negative contours are dashed: (a) first molecule; (b) second molecule.

Ab Initio Spin Density Calculation

Having obtained the accurate polarized neutron diffraction data, we performed several theoretical calculations to choose a method most suitable for spin density calculations in this kind of open-shell systems.

One family of *ab initio* methods aims to approach the Schrödinger equation solution for the electron system in the Born–Oppenheimer approximation. This family includes the classical unrestricted Hartree–Fock (UHF) method, its extensions which take into account configuration interaction using the Moller–Plesset perturbation theory[26] (MP2, MP3, etc.), and methods which use the Ritz linear variation procedure to solve the Schrödinger equation—configuration interaction (CI).[27] When applying these methods to a particular problem, it is important to choose an appropriate basis set. Gaussian-type basis sets are very useful, since they allow efficient implementation of the self-consistent field procedure and analytic gradient calculations. These

(26) Moller, C.; Plesset, M. S. *Phys. Rev.* **1934**, *46*, 618.
(27) Shavitt, I. Methods of Configurational Interaction. In *Modern Theoretical Chemistry*; Shaefer, H. F., III, Ed.; Plenum Press: New York, 1977; Vol. 3, pp 189–267.

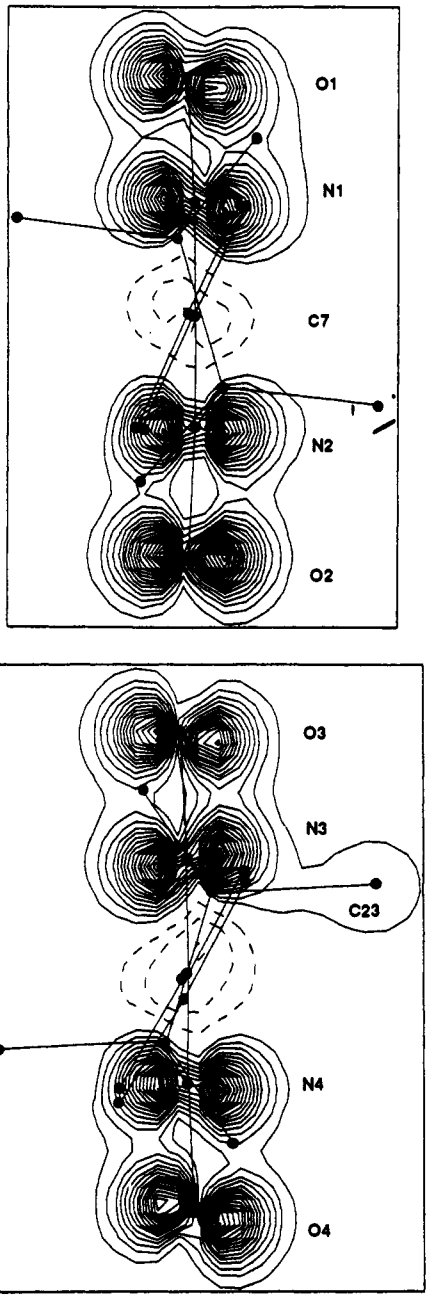

Figure 7. Projection onto a plane perpendicular to the nitroxide mean plane of the contours (step 0.04 $\mu_B/Å^2$) of the spin density as analyzed by wave-function modeling. The zero-level contour is not shown. Negative contours are dashed: (a) first molecule; (b) second molecule.

methods, particularly complete CI calculations, are very time-consuming. For this reason a truncated molecule was used in which the phenyl and methyl groups were replaced by hydrogen atoms. We performed several calculations using the GAUSSIAN 90/92[28] packages. We started with a simple UHF calculation using the rather small 3–21G basis set. The geometry was optimized in this calculation, and the obtained structural parameters are listed in Table 6. Unlike the structure of NitPh, the optimized truncated molecule is perfectly planar. This geometry was then used for all the other calculations. To understand the role of the basis set, another UHF calculation was performed in the huge 6–311G** basis set. To see how the result is influenced by the way configuration interaction is accounted for, MP2 and CI calculations in the 3–21G basis set were also carried out. These could be done only in the small basis set, since otherwise nonrealistic computational time would be required.

Table 6. Bond Lengths and Angles for the UHF 3-21G Optimized Geometry of a Truncated Molecule[a]

distance or angle	mean experimental	UHF 3-21G optimized
O–N	1.270(4) Å	1.284 Å
N–C(sp^2)	1.355(4) Å	1.348 Å
N–C(sp^3)		1.466 Å
C(sp^3)–C(sp^3)		1.535 Å
O–N–C(sp^2)	126.8(3)°	126.8°
O–N–C(sp^3)		122.0°
N–C(sp^2)–N	109.0(3)°	110.6°

[a] The optimized molecule is perfectly planar. Experimental values averaged over the two molecules are also shown for the O–N–C–N–O fragment.

As an alternative approach to first-principle calculation of the spin density, we have applied the density functional theory (DFT)[29] as implemented in the programs DGAUSS[30] and DMol.[31] At the local spin density functional level the functional of Vosko, Wilk, and Nusair (VWN)[32] was utilized. With DMol also the gradient-corrected (sometimes also referred to as nonlocal) spin density functional for exchange of Becke[33] was used. Since correlation is still according to the VWN functional, these calculations are referred to as B88VWN. Becke actually gives only the total energy functional; in the present work its functional derivative, which is the effective potential acting on the orbitals, has been used in the SCF iterations, as should be done in order to see its impact on the spin densities.

The DGAUSS program uses Gaussian basis sets. The calculations were done with local density optimized basis sets at the DZVP and TZVP levels for both the optimized geometry explained above and the complete NitPh molecule with the experimental geometry for the second molecule of the compound. The DMol program uses atomic-like basis sets[34] which recover the DFT dissociation limit exactly. Calculations with the two functionals mentioned above for the complete NitPh molecule have been done with a custom basis set which can be denoted as DNPP. This basis set uses all the functions of the standard basis file and has been shown to yield also excellent deformation densities[35,36] and other properties.[34,37-39]

The individual atomic spin populations for the O–N–C–N–O fragment calculated by various *ab initio* methods are listed in Table 7 together with experimental values. The latter are scaled to 1 μ_B/formula. Those resulting from UHF, MP2, and CI were obtained by integrating the three-dimensional spin density distribution in the vicinity of nuclear sites. Mulliken populations are given for DGAUSS, and those for DMol are integrals of partitioned atomic densities.[34] Table 8 shows the results of DGAUSS calculations for the complete molecule.

Discussion

In the studied $P2_1/c$ form of NitPh there are two crystallographically independent molecules of the radical. Although this

(28) (a) Frisch, M. J.; Head-Gordon, M.; Trucks, G. W.; Foresman, J. B.; Schlegel, H. B.; Raghavachari, K.; Robb, M. A.; Binkley, J. S.; Gonzalez, C.; DeFrees, D. J.; Fox, D. J.; Whiteside, R. A.; Seeger, R.; Melius, C. F.; Baker, J.; Martin, R. L.; Kahn, L. R.; Stewart, J. J. P.; Topiol, S.; Pople, J. A. *Gaussian 90*; Gaussian Inc.: Pittsburg, PA, 1990. (b) Frisch, M. J.; Trucks, G. W.; Head-Gordon, M.; Gill, P. M. W.; Wong, M. W.; Foresman, J. B.; Johnson, B. G.; Schlegel, H. B.; Robb, M. A.; Replogle, E. S.; Gomperts, R.; Andres, J. L.; Raghavachari, K.; Binkley, J. S.; Gonzalez, C.; Martin, R. L.; Fox, D. J.; DeFrees, D. J.; Baker, J.; Stewart, J. J. P.; Pople, J. A. *Gaussian 92*; Gaussian Inc.: Pittsburg, PA, 1992.

(29) Kohn, W.; Sham, L. J. *Phys. Rev.* **1965**, *140*, A1133.

(30) UniChem DGauss 1.1, Cray Research Inc., Cray Research Park, 655 Lone Oak Drive, Eagan, MN 55121.

(31) DMol, Biosym Technologies Inc., 9686 Scranton Road, San Diego, CA 92121–2777.

(32) Vosko, S. H.; Wilk, L.; Nausair, M. *Can J. Phys.* **1980**, *58*, 1200.

(33) Becke, A. D. *Phys. Rev.* **1988**, *A38*, 3098.

(34) Delley, B. *J. Chem. Phys.* **1990**, *92*, 508. Delley, B. *J. Chem. Phys.* **1991**, *94*, 7245.

(35) Delley, B. *Chem. Phys.* **1986**, *110*, 329.

(36) Moeckly, P.; Schwarzenbach, D.; Burgi, H.-B.; Hauser, J.; Delley, B. *Acta Crystallogr.* **1988**, *B44*, 636.

(37) Delley, B. *Physica B* **1991**, *172*, 185.

(38) Delley, B. *New J. Chem.* **1992**, *16*, 1103.

(39) Delley, B.; Steigmeier, E. F. *Phys. Rev. B* **1992**, *16*, 1103.

Table 7. Experimental and Theoretical Atomic Spin Populations for the O–N–C–N–O Fragment[a]

site	UHF 3-21G	UHF 6-311G**	MP2 3-21G	CI 3-21G	VWN[a] DZVP	VWN[a] TZVP	VWN[b] DNPP	B88VWN[b] DNPP	experiment
O	0.50	0.40	0.32	0.39	0.32	0.30	0.29	0.29	0.27
N	0.27	0.36	0.34	0.23	0.21	0.22	0.20	0.21	0.27
C(sp^2)	−0.55	−0.52	−0.31	−0.24	−0.08	−0.07	−0.02	−0.04	−0.11

[a] Experimental values are averaged over the two molecules and the two NO groups within each molecule. They are scaled to yield 1 μ_B per NitPh formula. DFT calculations were performed using the (a) DGAUSS and (b) DMOL programs.

Table 8. DFT (DGAUSS) Theoretical Atomic Spin Populations Calculated for the Experimental Geometry of the Second NitPh Molecule in Comparison with Experimental Values scaled to yield 1 μ_B per NitPh formula

site	experiment	DFT
O4	0.277(13)	0.319
N4	0.278(15)	0.238
C20	−0.121(17)	−0.065
N3	0.278(16)	0.210
O3	0.247(13)	0.288
C21	−0.025(16)	−0.004
C22	0.009(13)	−0.005
C23	0.055(12)	0.021
C24	0.009(13)	0.000
C25	−0.008(12)	0.001
C26	−0.005(13)	0.023
C15	0.000(13)	−0.009
C16	0.025(13)	0.002
C17	−0.016(12)	−0.009
C18	0.011(12)	0.002
C19	−0.037(13)	−0.009
C14	0.024(16)	0.004

situation could have led to an overparametrized problem, a large and precise set of data has been collected and the presence of two independent molecules gives the opportunity to check the reliability of our experiment. Nearly identical spin distributions are obtained for both molecules, so that the results can be confidently discussed on the quantitative level.

Most of the spin density is concentrated on the nitronyl nitroxide ring and is located on the NO groups in a π^* orbital. Although this result corresponds to the familiar picture predicted by elementary molecular orbital theory, our study brings additional quantitative information. (i) Within each molecule both NO groups carry equal spin density. Furthermore, this density is equally shared by the oxygen and nitrogen atoms within each NO group, as previously observed in piperidinyl nitroxides.[40] (ii) The spin distribution features a large negative-spin population of the sp^2 carbon atom bridging the two NO groups (C7 and C20). (iii) Weak alternating ...+/−/+/−... contributions from the phenyl ring carbon atoms are observed. They are often at the limit of the experimental accuracy. Nevertheless, sign alternation and even their magnitudes are in good agreement with those resulting from ^1H and ^{13}C NMR experimental investigations.[41,42]

Thus spin polarization effects are confirmed in these π free radicals. The presence of carbon sites carrying spin densities of opposite sign may allow for intermolecular coupling involving nonorthogonal orbitals, leading to ferromagnetic interaction. Such mechanisms depend on crystal packing and are not efficient in NitPh, but they probably play a major role in determining bulk ferromagnetism in related nitroxides.[43]

The present results are worth being compared with the recently reported spin density distribution in a NitPh coordinated to metal ions.[10] In the coordinated species the spin density is unevenly shared by the oxygen and nitrogen atoms of the bound NO group. Depending on the coordination mode and the magnitude of the metal–nitroxyl magnetic interaction, the spin density on the bound oxygen is modified and may completely vanish. In giving identical populations to both atoms of the NO groups, the present study affords definite proof of the reorganization of the spin distribution upon coordination and brings strong support to the proposed participation of the ionic Lewis structure of the nitroxyl group in metal complexes.

In spite of the strong modification of the spin distribution on nitrogen and oxygen atoms, the negative spin density on the sp^2 carbon atoms bridging the NO groups is also present in the coordinated case. The magnitude of this negative population remains equal to approximately one third of averaged (now different) N and O populations, as found in the isolated species. Thus the reorganization of the spin distribution does not affect the polarization of sp^2 carbon atoms.

Extrapolation of the observed weak contributions of the phenyl carbons to pyridine-substituted nitroxides leads to the expectation that coupling pathways through the aromatic substituent will not be very efficient. Indeed in a series of metal complexes derived from the 4-pyridyl-substituted ligand, it has been observed that the interaction mediated by the substituent is at least 1 order of magnitude weaker than that corresponding to direct ligation of the nitroxyl group.

One can now compare the results of *ab initio* calculations to those obtained experimentally. All the calculations give correct signs of spin populations. They differ however in how well they manage to predict the magnitudes of populations. The main discrepancies are the disproportion between O and N populations (which are found to be equal experimentally) and the amount of negative spin on the bridging C atom. In comparing different *ab initio* methods, two aspects should be considered.

(i) The calculations differ in the way they take into account the correlation energy. UHF calculations are never able to achieve the exact solution of the Schrödinger equation, since they completely neglect the correlations. The UHF calculation in the 3–21G basis set gives a strong O/N disproportion and severely exaggerates the spin polarization effect on the bridging carbon. MP2 calculations can approach the exact solution much closer, since usually the correlation energies are rather small and the perturbation treatment is justified. Even with the small basis set, a good O/N ratio is obtained. The spin polarization effect is still exaggerated. In principle, a 'full' CI calculation should be able to find an exact solution of the Schrödinger equation. But in our case CI results are surprisingly poor, even though, among all the methods discussed above, CI gives the best value for negative spin density on C, only twice the experimental value.

(ii) The calculations may differ in the size of basis set which they use. An improvement of the O/N ratio is observed when using the large 6321-G** basis set instead of the small 3–21G one for UHF. This illustrates that a good basis choice is crucial for this technique. The insufficiency of the basis set also explains the low quality of CI results. In a finite basis set, only a projection of the true Hamiltonian is used. To obtain reliable spin populations, a very large basis set is probably required. This cannot be practically implemented, since the computational time for such a calculation would be tremendous.

The results obtained by density functional calculations are the most satisfactory. They seem to be very stable with respect to the choice of basis and the actual functional used. The computational time is much smaller than that for other methods.

(40) Bordeaux, D.; Boucherle, J. X.; Delley, B.; Gillon, B.; Ressouche, E.; Schweizer, J. In *Magnetic Molecular Materials*; Gatteschi et al., Eds.; NATO ASI Series; Kluwer: Dordrecht, The Netherlands, 1991; Vol. 198, pp 371–384.

(41) Davis, M. S.; Morokuma, K.; Kreilick, R. W. *J. Am. Chem. Soc.* **1972**, *94*, 5588.

(42) Neely, J. W.; Hatch, G. F.; Kreilick, R. W. *J. Am. Chem. Soc.* **1974**, *96*, 652.

(43) Awaga, K.; Maruyama, Y. *J. Chem. Phys.* **1989**, *91*, 2743.

The difference between the obtained O/N population ratio (~3:2) and the experimental value (1:1) is approximately the same as that found by UHF calculations, but only the DFT methods give a sufficiently small spin polarization effect on the central carbon atom. Only these methods are fast enough to permit calculations for a complete NitPh molecule, predicting the alternating populations on the phenyl fragment observed experimentally. It is notable that the main features of the calculated spin density hardly change when going from idealized to real geometry. This suggests that our comparison of experimental populations and those obtained theoretically for a simplified molecule is meaningful. Contrary to UHF and different levels of configuration interaction treatments, DFT does not exaggerate the spin polarization effect, as previously demonstrated for other organic free radicals.[44-46] Since sites with negative spin densities are crucial for some organic ferromagnet design strategies, this fact is a strong argument in favor of the DFT *ab initio* approach.

Conclusion

The polarized neutron diffraction determination of the spin distribution in a phenyl-substituted nitronyl nitroxide free radical has been performed. The high-quality data obtained in this experiment allowed us to reconstruct the spin density using an *a priori* model and giving direct experimental evidence for the p-shape of the magnetic orbital in the vicinity of the main spin-carrying atoms.

The spin density is mainly concentrated on the two NO groups. In contrast to the cases were an analogous molecule is involved in a metal complex, it is equally shared by the four atoms. In all the cases, the spin density on the carbon atom bridging the two NO groups is negative and significant.

Finally, comparison of the available theoretical methods shows that the most stable, fast, and reliable technique calculations of spin densities is the DFT approach.

Supplementary Material Available: Labeling of all atoms including hydrogen (Figure S1), picture showing the positions of the NitPh molecules with respect to the unit cell (Figure S2), tables of atomic fractional cell coordinates and isotropic thermal parameters (Table S1) and bond lengths and angles (Tables S2 and S3) (7 pages). This material is contained in many libraries on microfiche, immediately follows this article in the microfilm version of the journal, and can be ordered from the ACS; see any current masthead page for ordering information.

(44) Zheludev, A.; Grand, A.; Ressouche, E.; Schweizer, J.; Morin, B.; Epstein, A. J.; Dixon, D.; Miller, J. S. Spin density in the Tetracyanoethylenide Free Radical Ion. In preparation.

(45) Bordeaux, D.; Boucherle, J. X.; Delley, B.; Gillon, B.; Ressouche, E.; Schweizer, J. *Z. Naturforsch.* **1992**, *48A*, 117.

(46) Delley, B.; Becker, P.; Gillon, B. *J. Chem. Phys.* **1984**, *80*, 4286.